Applied Physics Letters

PERSPECTIVE | JULY 01 2021

Toward the predictive discovery of ambipolarly dopable ultra-wide-band-gap semiconductors: The case of rutile GeO_2

Sieun Chae; Kelsey Mengle ; Kyle Bushick ; Jihang Lee; Nocona Sanders; Zihao Deng ; Zetian Mi ; Pierre F. P. Poudeu ; Hanjong Paik ; John T. Heron ; Emmanouil Kioupakis

Appl. Phys. Lett. 118, 260501 (2021)
https://doi.org/10.1063/5.0056674

AIP Publishing

Applied Physics Letters PERSPECTIVE scitation.org/journal/apl

Toward the predictive discovery of ambipolarly dopable ultra-wide-band-gap semiconductors: The case of rutile GeO_2

Cite as: Appl. Phys. Lett. **118**, 260501 (2021); doi: 10.1063/5.0056674
Submitted: 12 May 2021 · Accepted: 3 June 2021 ·
Published Online: 1 July 2021

View Online Export Citation CrossMark

Sieun Chae,[1] Kelsey Mengle,[1] Kyle Bushick,[1] Jihang Lee,[1] Nocona Sanders,[1] Zihao Deng,[1] Zetian Mi,[2] Pierre F. P. Poudeu,[1] Hanjong Paik,[3] John T. Heron,[1,a)] and Emmanouil Kioupakis[1,a)]

AFFILIATIONS

[1]Department of Materials Science and Engineering, University of Michigan, Ann Arbor, Michigan 48109, USA
[2]Department of Electrical and Computer Engineering, University of Michigan, Ann Arbor, Michigan 48109, USA
[3]Platform for the Accelerated Realization, Analysis, and Discovery of Interface Materials (PARADIM), Cornell University, Ithaca, New York 14853, USA

[a)]Authors to whom correspondence should be addressed: jtheron@umich.edu and kioup@umich.edu

ABSTRACT

Ultrawide-band-gap (UWBG) semiconductors are promising for fast, compact, and energy-efficient power-electronics devices. Their wider band gaps result in higher breakdown electric fields that enable high-power switching with a lower energy loss. Yet, the leading UWBG semiconductors suffer from intrinsic materials' limitations with regard to their doping asymmetry that impedes their adoption in CMOS technology. Improvements in the ambipolar doping of UWBG materials will enable a wider range of applications in power electronics as well as deep-UV optoelectronics. These advances can be accomplished through theoretical insights on the limitations of current UWBG materials coupled with the computational prediction and experimental demonstration of alternative UWBG semiconductor materials with improved doping and transport properties. As an example, we discuss the case of rutile GeO_2 (r-GeO_2), a water-insoluble GeO_2 polytype, which is theoretically predicted to combine an ultra-wide gap with ambipolar dopability, high carrier mobilities, and a higher thermal conductivity than β-Ga_2O_3. The subsequent realization of single-crystalline r-GeO_2 thin films by molecular beam epitaxy provides the opportunity to realize r-GeO_2 for electronic applications. Future efforts toward the predictive discovery and design of new UWBG semiconductors include advances in first-principles theory and high-performance computing software, as well as the demonstration of controlled doping in high-quality thin films with lower dislocation densities and optimized film properties.

INTRODUCTION

Modern semiconductor device technology advances with the development of new semiconducting materials. Commercial semiconductors, such as Si, Ge, and the III-V families (e.g., nitrides, phosphides, arsenides, etc.), are both n-type and p-type dopable, which enables a wide variety of devices such as visible light-emitting diodes and field-effect transistors. For efficient high-power electrical conversion and UV light emission, however, ultrawide-band-gap (UWBG) semiconductors with gaps wider than the 3.4 eV gap of GaN are necessary. AlN and high-Al-content AlGaN, β-Ga_2O_3, diamond, and c-BN have all emerged as candidate materials to advance the frontier in high-power electronics.[1] The Baliga figure of merit (BFOM $= \frac{1}{4}\varepsilon_0\mu E_c^3$, where ε_0 is the static dielectric constant, μ is the carrier mobility, and E_c is the dielectric breakdown field) is commonly used to quantify the interplay between the breakdown voltage and energy dissipation through resistive losses and thus to benchmark the efficiency of materials for power devices. Table I lists the BFOM and thermal conductivity for current state-of-the-art UWBG materials. Due to the cubic dependence of the BFOM on the dielectric breakdown field, the most promising materials are those with band gaps wider than 3.4 eV.

The emerging UWBG materials face several doping challenges, however. Specifically, ambipolar doping is a challenge for all current UWBG materials, which limits the application of many UWBG semiconductors to unipolar devices. For $Al_xGa_{1-x}N$, both n-type and p-type doping efficiencies decrease with increasing Al content, x, as the ionization energy of the Mg acceptor increases and compensating defects, such as N vacancies, form more easily with increasing x.[32,33] β-Ga_2O_3 is characterized by flat valence bands that lead to deep

TABLE I. Baliga's figure of merit (BFOM $= \frac{1}{4}\varepsilon_0\mu E_C^3$) and thermal conductivity for silicon and common ultra-wide-band-gap semiconductors. ε_0 is the static dielectric constant, μ_e/μ_h is the electron/hole mobility at room temperature, E_C is the dielectric breakdown field predicted based on the breakdown vs band gap relation established by Higashiwaki *et al.*,[2] E_d/E_a is the donor/acceptor ionization energy, and κ is the thermal conductivity at room temperature. μ_e/μ_h is the experimental maximum realized values for all materials except r-GeO_2, whereas μ_e/μ_h of r-GeO_2 is phonon-limited mobility calculated by the density functional theory (DFT).

Material	ε_0	μ_e/μ_h ($cm^2\ V^{-1}\ s^{-1}$)	E_C ($MV\ cm^{-1}$)	E_d/E_a (eV)	n-/p-BFOM ($10^6\ V^2\ \Omega^{-1}\ cm^{-2}$)	κ ($W\ m^{-1}\ K^{-1}$)
Si	11.9[3]	1240[4]/450[5]	0.3[2]	0.04/0.05[6]	8.8[7]/3.2	130[6]
4H-SiC	9.7[4]	980[4]/120[8]	2.5[2]	0.05/0.19[9]	3300[7]/404	370[1]
GaN	10.4 (‖c)[10]	1000[8]/31[11]	3.3[2]	0.04/0.21[12]	8300/257[7]	253[1]
β-Ga_2O_3	10.0[13]	184[14]/-	6.4[2]	0.04[15]/1.1[16]	6300[7]/-	11; 27[17]
AlN	9.1[18]	426[19]/14[20]	15.4[1]	0.25[21]/1.4[20]	336 000[1]/11 000	286; 319[22]
c-BN	7.1[23]	200[23]/500[24]	17.5[1]	0.15[25]/0.24[26]	27 800/695 000[1]	1600[27]
Diamond	5.7[6]	1060/2000[28]	13.0[1]	0.57/0.38[28]	294 000/554 000[1]	2290–3450[28]
r-GeO_2	14.5 (⊥c)[29]	244/27[7]	7.0[7]	<0.04/0.45[30]	27 000/3000[7]	51[31]
	12.2 (‖c)[29]	377/29[7]			35 000/2700[7]	

ionization energies for acceptors (>1.1 eV) and the formation of self-trapped hole polarons.[16,34] For c-BN and diamond, n-type doping has proven to be challenging. Due to the small lattice constant of c-BN and diamond, the range of dopants that fit into the lattice is severely limited, and the best substitutional donors (currently P for diamond, and S and Si for c-BN) have high activation energies (>0.4 eV).[35–37]

Additionally, each of the current UWBG materials has its own drawbacks that hamper its adoption in devices. AlGaN and diamond suffer from high synthesis and processing costs, high dislocation densities, and limited size of native substrates. The synthesis of c-BN is also challenging as the hexagonal phase of BN is more stable than the cubic polytype. β-Ga_2O_3 is currently the subject of intense research activity due to the availability of affordable semi-insulating native substrates and the ease of n-type doping. However, β-Ga_2O_3-based devices are energy-inefficient owing to the relatively low mobility ($184\ cm^2\ V^{-1}\ s^{-1}$)[14] compared to other UWBG semiconductors, while its poor thermal conductivity ($11\ W\ m^{-1}\ K^{-1} \parallel \vec{a}$ and $27\ W\ m^{-1}\ K^{-1} \parallel \vec{b}$)[17] hinders the removal of the generated heat. Therefore, UWBG semiconductor research must simultaneously seek to improve the performance of current materials in order to realize their full potential, and at the same time to explore novel UWBG materials and critically assess their potential to advance the current state of the art.

In the exploration of new materials, a number of prospective UWBG materials have been proposed. For example, recent calculations have identified that the rocksalt phase of ZnO is ambipolarly dopable.[38] However, rocksalt ZnO is metastable and has been stabilized only by alloying it with other rocksalt oxides (e.g., NiO or MgO), which sacrifices the mobility and/or doping properties.[39] Spinel $ZnGa_2O_4$ has proven to be n-type dopable with a band gap and electron mobility comparable to β-Ga_2O_3.[40] Hole conduction, however, has been achieved only at high temperatures (>600 K),[41] while the thermal conductivity is also low ($22.1\ W\ m^{-1}\ K^{-1}$)[40]. $LiGaO_2$ is also a potential ultrawide-band-gap (5.8 eV) semiconductor, which is theoretically predicted to be n-type dopable with Si or Ge, though experimental investigation is needed to realize its potential application.[42–44]

In our recent work, we identified rutile GeO_2 (r-GeO_2) as a promising UWBG ($E_g = 4.68$ eV) semiconductor with ambipolar dopability, high thermal conductivity, and high BFOM (Table I). Furthermore, the stabilization of single-crystalline r-GeO_2 bulk crystals and thin films makes experimental investigations feasible. In this Perspective, we review the key properties of r-GeO_2 as an UWBG semiconductor, and we articulate challenges and opportunities for the field.

R-GeO_2 CRYSTAL STRUCTURE, BAND STRUCTURE, AND EFFECTIVE MASSES

In the periodic table, Ge is the group 14 element between Si and Sn, sitting in the fourth period next to Ga. Accordingly, GeO_2 has an ultra-wide band gap similar to that of Ga_2O_3 but adopts chemical and structural properties analogous to SiO_2 or SnO_2. Though both Ga_2O_3 and SnO_2 are established wide-band-gap n-type semiconductors, a little has been known about the semiconducting properties of GeO_2 until recently. Among the multiple polymorphs of GeO_2, the octahedrally coordinated rutile structure is the high-density crystalline polytype and the thermodynamically most stable phase up to 1030 °C.[45] In contrast to quartz or amorphous GeO_2, the rutile phase is insoluble in water,[46] thus it is better suited for device processing.

The crystal structure of rutile GeO_2 (r-GeO_2) is shown in Fig. 1(a). Considering the anisotropy of the rutile crystal structure, its optical or transport properties are often studied along different crystallographic directions (e.g., ⊥ c and ‖ c). The electronic band structure of r-GeO_2 is calculated using different methods such as the local density approximation (LDA),[47] the generalized gradient approximation (GGA),[48] the Heyd-Scuseria-Ernzerhof (HSE06) hybrid functional,[30] and G_0W_0.[49,50] The G_0W_0-calculated quasiparticle band structure of r-GeO_2 is presented in Fig. 1(b). The fundamental band gap of r-GeO_2 is direct at Γ, with a calculated value (4.44 eV) that is close to experimental UV-absorption measurements (4.68 eV).[51] The direct optical gap between the VBM and CBM is dipole forbidden, and the direct allowed transitions occur from VBs approximately 0.6 eV (2.21 eV) below valence-band maximum (VBM) and the conduction-band minimum (CBM) for the ⊥ c (‖ c) direction (Table III in Ref. 49). This band-gap value falls into the UWBG region, making r-GeO_2 promising for power electronics applications.

Another band feature is the band dispersion, i.e., the effective mass (m^*). The carrier effective masses are key parameters that determine the n-/p-type dopability, since according to the Bohr model, the shallow donor/acceptor ionization energy ($E_{d/a}$) is proportional to the

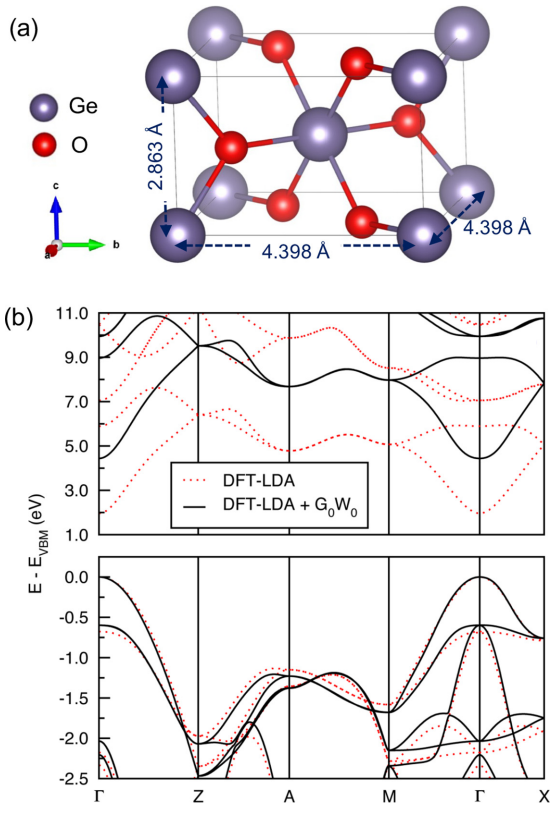

FIG. 1. (a) Crystal structure and (b) the electronic band structure of r-GeO_2 calculated within DFT-LDA (red dotted lines) and with the quasiparticle DFT-LDA + G_0W_0 method (black solid lines). Reproduced from Mengle *et al.*, J. Appl. Phys. **126**, 085703 (2019) with the permission of AIP Publishing.

electron/hole effective mass ($E_{d/a} = 13.6 \cdot \frac{m^*_{e/h}}{\varepsilon_r^2}$ eV). The Drude mobility ($\mu = \frac{e \cdot \tau}{m^*}$) and the coupling constant of polarons are also determined by m^*,[52] thus lighter effective masses improve the electrical conductivity of semiconductors and suppress the formation of polarons in polar materials. However, the effective mass generally becomes heavier as the band gap increases,[52] which makes most UWBG materials unsuitable for electronic applications.

Despite its ultra-wide band gap, r-GeO_2 exhibits relatively a light electron and hole effective masses. The effective-mass values of r-GeO_2 are obtained by fitting the hyperbolic equation to the G_0W_0 band structure. The electron effective masses along $\Gamma \rightarrow X$ ($m^*_{e\perp}$) and $\Gamma \rightarrow Z$ ($m^*_{e\parallel}$) are 0.43 m_0 and 0.23 m_0, respectively.[49] These values are similar to other n-type semiconductors such as β-Ga_2O_3 (0.23–0.34 m_0),[53] SnO_2 (0.23–0.30 m_0),[54] and GaN (0.19–0.21 m_0).[55] In addition, the hole effective masses ($m^*_{h\perp}$=1.28 m_0 and $m^*_{h\parallel}$=1.74 m_0[49]) are notably small compared to other common ultra-wide-band-gap materials. For β-Ga_2O_3, the valence band is notoriously flat,[56] resulting in a large hole effective mass of ~40 m_0, which also gives rise to trapped hole polarons with a trapping energy of 0.53 eV.[34] In contrast, in the absence of impurities, the self-trapped energy of hole polaron in r-GeO_2 is calculated to be less than 0.01 eV,[49] indicating its superior hole-transport properties compared to β-Ga_2O_3.

Why are the effective masses of r-GeO_2 lower than materials with similar band gaps? First, the conduction bands consist of delocalized Ge 4*s* orbitals, leading to a broad conduction band width. Moreover, while the top valence bands consist of localized O 2*p* orbitals, the densely packed oxygen atoms allow holes to conduct easily through oxygen orbitals. The delocalized nature of electrons and holes makes r-GeO_2 promising for ambipolar dopability.

DONORS AND ACCEPTORS

To identify potential donors and acceptors in r-GeO_2, Chae and colleagues have applied the hybrid density functional theory to calculate the formation and ionization energies of dopants and to identify possible sources of charge compensation.[30] From the calculations, it is predicted that Sb_{Ge}, As_{Ge}, and F_O are all shallow donors with an ionization energy of ~25 meV [Figs. 2(a) and 2(b)]. The incorporation of donors varies depending on the growth conditions: F_O is favored under O-poor/Ge-rich growth, while Sb_{Ge} is the donor with the lowest formation energy under O-rich/Ge-poor conditions. Under O-rich/Ge-poor conditions, however, the Ge vacancy is an unavoidable defect that compensates donors. Therefore, O-poor/Ge-rich growth conditions are preferred to enable n-type doping under thermodynamic equilibrium, since the only compensating defects we identified are

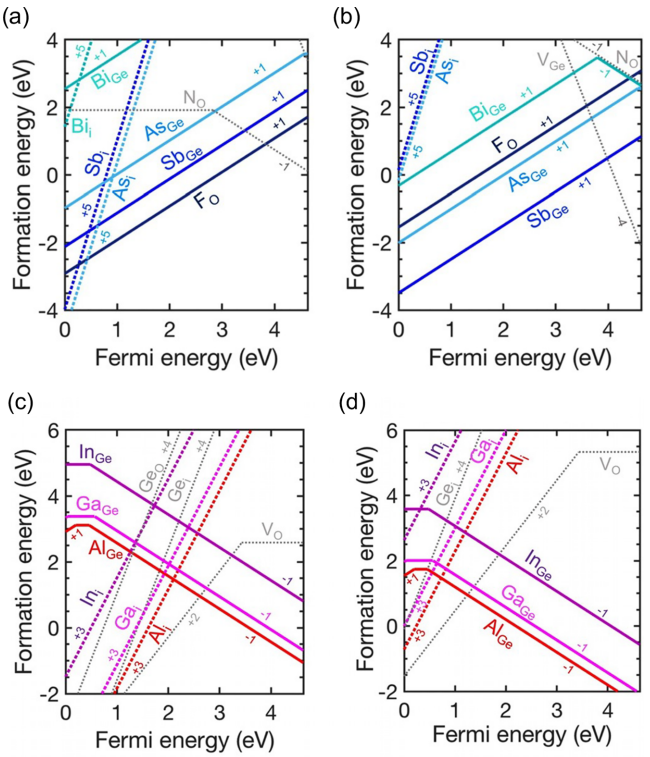

FIG. 2. Formation energy of (a) and (b) donor defects and (c) and (d) acceptor defects along with potential charge-compensating native defects as a function of the Fermi level. The simulated growth conditions are (a) and (c) Ge rich/O poor and (b) and (d) O rich/Ge poor conditions. Reproduced from Chae *et al.*, Appl. Phys. Lett. **114**, 102104 (2019) with the permission of AIP Publishing.

nitrogen impurities (N_O), which, however, can be eliminated by excluding N from the growth environment.

Group 13 elements, such as Al, Ga, and In, are possible acceptors in r-GeO_2, among which Al_{Ge} is calculated to be the best candidate acceptor due to its low ionization energy and low formation energy [Figs. 2(c) and 2(d)]. While hole polarons do not form in the absence of impurities, all acceptors examined in the study form a hole polaron in the neutral charge state accompanied by local lattice distortions, resulting in a relatively high ionization energy (0.45 eV for Al_{Ge}). Also, charge compensation from donor-type native defects such as V_O or self-passivating defects (Al_i) can be a challenge for p-doping of r-GeO_2. However, due to the strong Coulombic interaction between Al_{Ge} and hydrogen interstitial (H_i), co-doping with H_i can effectively enhance the solubility of Al_{Ge} up to the Mott-transition limit ($\sim 10^{20}\,cm^{-3}$), allowing an impurity band to form and reducing the effective ionization energy. P-type conduction is enabled through the impurity band by post-annealing removal of H_i to activate hole carriers. Thermally activated p-type conduction of r-GeO_2 has also been demonstrated experimentally by Niedermeier *et al.*[57] The notably shallow acceptor ionization of r-GeO_2 compared to other established WBG oxide semiconductors (e.g., 0.91 eV for SnO_2[58]) originates from the dense network of O atoms in r-GeO_2 that allows strong O 2*p* antibonding interactions and leads to a high-lying VBM (see the supplementary material of Refs. 30 and 57) and light hole effective masses. This is in contrast to the valence bands of most oxide semiconductors that are deep (thus inducing high ionization potentials).

MOBILITY, BFOM, AND THERMAL CONDUCTIVITY

For energy-efficient power electronic devices, a high carrier mobility (μ) for efficient carrier transport, a high breakdown field (E_C) and dielectric constant (ε_0) for high voltage operation, and a high thermal conductivity (κ) for efficient heat extraction are necessary. Bushick *et al.*[7] determined the phonon-limited electron and hole mobilities of r-GeO_2 as a function of temperature and crystallographic orientation by applying density functional and density functional perturbation theories to calculate carrier-phonon coupling in r-GeO_2 [Figs. 3(a) and 3(b)]. At 300 K, the calculated electron mobilities are $\mu_{elec,\perp\vec{c}} = 244\,cm^2\,V^{-1}\,s^{-1}$ and $\mu_{elec,\parallel\vec{c}} = 377\,cm^2$, and the calculated hole mobilities are $\mu_{hole,\perp\vec{c}} = 27\,cm^2\,V^{-1}\,s^{-1}$ and $\mu_{hole,\parallel\vec{c}} = 29\,cm^2\,V^{-1}\,s^{-1}$. The polar-optical modes exhibit the strongest carrier-phonon coupling, and the low-energy polar-optical modes limit the room-temperature mobility in r-GeO_2. The calculated electron mobility is comparable to currently used n-type semiconductors. Also, the hole mobility or r-GeO_2 is comparable to that of p-type GaN, again showing its promising properties for p-type conduction.

Further computational and experimental results also point to favorable thermal properties for r-GeO_2. Figure 3(c) shows the theoretically predicted and the experimentally measured thermal conductivity of r-GeO_2 as a function of temperature.[31] First-principles calculations predict an anisotropic phonon-limited thermal conductivity of $37\,W\,m^{-1}\,K^{-1}$ ($\perp$c) and $57\,W\,m^{-1}\,K^{-1}$ ($\parallel$c) at 300 K. Experimentally, the thermal conductivity was measured using the laser-flash method for hot-pressed, polycrystalline r-GeO_2 pellets with grain sizes of $\sim$1.50 μm. The measured value for r-GeO_2 ($51\,W\,m^{-1}\,K^{-1}$ at 300 K) is approximately two times higher than the highest value of β-Ga_2O_3 (11 and $27\,W\,m^{-1}\,K^{-1}$ along the $\vec{a}$ and $\vec{b}$ directions, respectively). Also, while β-Ga_2O_3 can be only grown on thermally insulating substrates (e.g., Al_2O_3), the higher symmetry of r-GeO_2 allows it to be epitaxially grown on thermally conductive materials such as SnO_2 ($100\,W\,m^{-1}\,K^{-1}$).[31]

By combining the calculated results for the mobility and dielectric constant, the BFOM of r-GeO_2 can be evaluated in Table I by using a breakdown field extracted from the breakdown field vs a band gap relation established by Higashiwaki *et al.*[2] While common ultra-wide-band-gap materials suffer from doping asymmetry, r-GeO_2 has relatively low dopant ionization energies for both donors and acceptors, and in combination with a higher thermal conductivity and a higher BFOM compared to β-Ga_2O_3, the results demonstrate the promise of r-GeO_2 to advance the state of the art in UWBG semiconductor device technology.

TOWARD EXPERIMENTAL DEMONSTRATION

To date, experimental reports on r-GeO_2 are largely focused on its synthesis.[60–65] Here, we summarize the current advances and challenges of r-GeO_2 synthesis. The rutile polymorph of GeO_2, with Ge^{4+} ions in the octahedral coordination, is the thermodynamically stable phase at ambient pressure and temperature [Fig. 4(a)]. R-GeO_2 transforms to the quartz phase (Ge^{4+} in the tetrahedral coordination) above 1000 °C and before melting.[46] Unlike SiO_2 and SnO_2, however, which are stable in the quartz and rutile structures, respectively, both the quartz and the rutile are deeply stable polymorphs of GeO_2 under

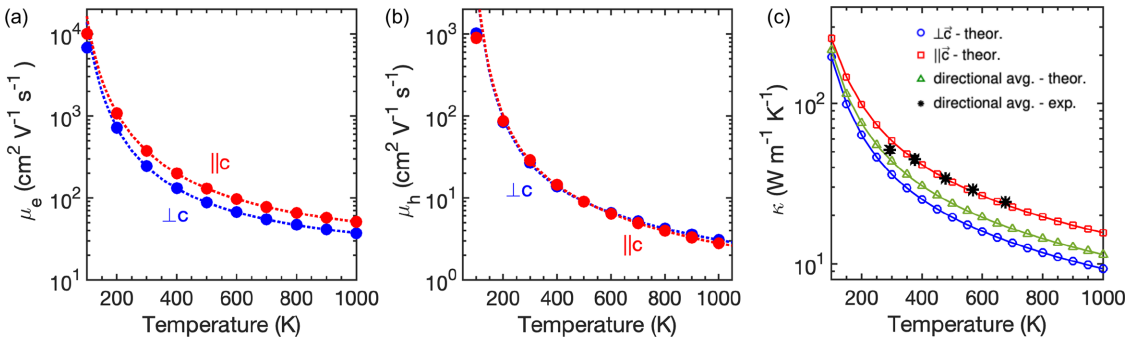

FIG. 3. (a) Phonon-limited electron and (b) hole mobility of r-GeO_2 along the $\perp$ c and $\parallel$ c directions as a function of temperature for a carrier concentration of $n = 10^{17}\,cm^{-3}$. Data from Ref. 59. (c) The theoretically calculated and experimentally measured thermal conductivity of polycrystalline r-GeO_2 from 100 to 1000 K. Reproduced from Chae *et al.*, Appl. Phys. Lett. **117**, 102106 (2020) with the permission of AIP Publishing.

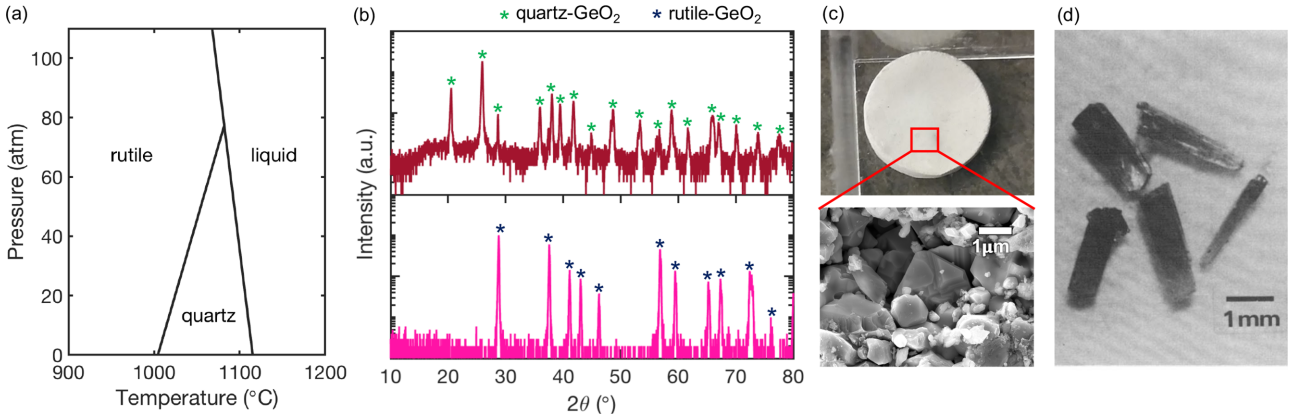

FIG. 4. (a) Phase diagram of GeO_2. The rutile is the most stable polytype under ambient conditions. (b) The x-ray diffraction of (top) GeO_2 powder and (bottom) a GeO_2 pellet after hot pressing (800 °C, 100 MPa) and subsequent annealing (1000 °C, air). (c) A digital image and a scanning electron microscope image of a hot-pressed GeO_2 pellet. (d) Single crystals of r-GeO_2 synthesized by chemical vapor transport. Panel (a) is adapted with permission from Hill and Chang., Am. Mineral. **53**, 1744 (1968). Copyright 1968 Mineralogical Society of America. Panels (b) and (c) are reproduced from Chae *et al.* Appl. Phys. Lett. **117**, 102106 (2020) with the permission of AIP Publishing. Panel (d) is adapted with permission from Agafonov *et al.*, Mater. Res. Bull. **19**, 233 (1984). Copyright 1984 Elsevier B. V.

ambient conditions.[45] Similarly to SiO_2, GeO_2 is also a glass former with a deeply metastable amorphous phase. Thus, one of the challenges in the synthesis of r-GeO_2 is navigating the kinetic and thermodynamic space to avoid the formation of the deleterious metastable quartz and amorphous phases.

The solid-state synthesis of r-GeO_2 can be achieved from commercially available quartz phase powder. As the phase transformation from quartz to rutile is accompanied by a large volume reduction of ~50% and must overcome a large energy barrier of ~400 kJ/mol, the phase transformation occurs with a pressure higher than 100 MPa and a temperature higher than 900 K (~0.45 T_m),[31,60,66] which can be achieved by hot pressing. Figure 4(b) shows x-ray diffraction data of the quartz-GeO_2 power precursor and subsequent r-GeO_2 pellets converted in a hot press.[31] The grain sizes of hot-pressed r-GeO_2 pellets range from 0.5 to 2 μ m [Fig. 4(c)]. At $T < 600K$ and $P > 6$ GPa conditions, a displacive transition occurs that changes the coordination of the Ge atom from four-fold to six-fold. The resulting phase is amorphous or distorted rutile, depending on the starting materials and pressing conditions.[61–63] While the synthesis of r-GeO_2 has been demonstrated through phase conversion, the small grain sizes are undesirable for modern power electronics as grain boundaries or voids act as charge-trapping or scattering centers and degrade the device performance.

Various bulk synthesis techniques have been attempted to realize r-GeO_2 single crystals. The melting temperature of GeO_2 is relatively low (1100 °C), and conventional crystal growth techniques from the melt [e.g., Czochralski (CZ) or float zone (FZ)] have successfully stabilized r-GeO_2. However, since quartz is the high-temperature stable solid phase, the solid-state phase change to the lower-temperature r-GeO_2 leads to significant internal cracking.[65] Instead, Goodrum[65] utilized alkali-oxide solvents to lower the liquidus temperature below the rutile-to-quartz transition temperature and reported the growth of 10 mm-long r-GeO_2 single crystals using the top-seeded flux technique. Single-crystal r-GeO_2 growth by chemical vapor transport is also reported [Fig. 4(d)].[64] Owing to the high vapor pressure of GeO_2, GeO molecules can easily desorb above 700 °C, and the re-condensation of these molecules has been successful for stabilizing the rutile phase. Agafonov *et al.*[64] utilized $TeCl_4$ and HCl as transport agents to carry GeO molecules and synthesized a single-crystal r-GeO_2 rod with a size of $0.5 \times 0.5 \times 2$ mm^3 using a temperature gradient of 1000–900 °C. These bulk synthesis studies have demonstrated the possibility of stabilizing bulk single crystals of GeO_2 in the rutile polymorph despite the existence of the competing quartz phase near the melting temperature. However, more studies are required to obtain highly crystalline large single crystals of r-GeO_2 that can be potentially used to produce substrates for the homoepitaxy of r-GeO_2 thin films aimed for electronic applications.

The thin-film growth of r-GeO_2 is challenging owing to the presence of the deeply metastable glass phase and the high vapor pressure of GeO_2. Prior works report the growth of GeO_2 films using sputtering,[67–70] pulse laser deposition,[71–73] and thermal evaporation,[74] but the as-deposited films are all amorphous, indicating a strong tendency for glass formation. Recently, however, epitaxial single-crystalline thin films of r-GeO_2 were successfully synthesized using ozone-assisted molecular beam epitaxy (MBE)[75] on R-plane sapphire. The R-plane sapphire is a suitable substrate for rutile oxide thin films due to the rectangular surface symmetry and the edge-sharing connectivity of the oxygen octahedra. Figure 5(a) shows the x-ray diffraction of r-GeO_2 thin films grown on (Sn,Ge)O_2/SnO_2 buffered sapphire substrates. In agreement with prior SnO_2 thin-film growth,[76–78] the in-plane registry is [010] GeO_2 || [11$\bar{2}$0] Al_2O_3 and [$\bar{1}$01] GeO_2 || [$\bar{1}$101] Al_2O_3.

It was found that the stabilization of single-crystalline rutile films requires a balance of epitaxial strain, adatom mobility, GeO desorption, and chemical composition. A compositional dependence of the (Sn,Ge)O_2 buffer layer on the stabilization of the r-GeO_2 film shows that a strain of 4.4% || [010] and 5.0% || [$\bar{1}$01] yields single-crystalline films, whereas a strain of 4.8% || [010] and 5.8% || [$\bar{1}$01] causes amorphization. Furthermore, the substrate temperature and ozone pressure must be optimized to allow sufficient adatom mobility without high desorption as well as to achieve proper stoichiometry. Single-crystalline films were realized in a narrow region of the growth-parameter space using a preoxidized molecular source to balance the

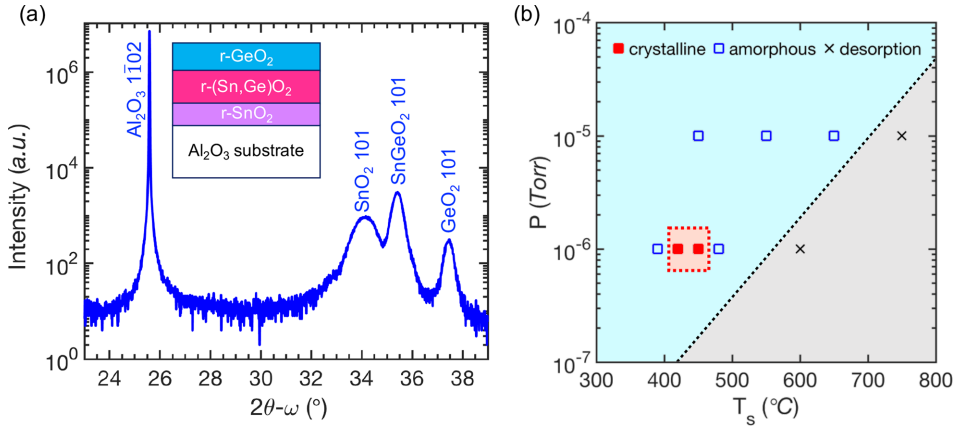

FIG. 5. (a) The x-ray diffraction of r-GeO_2 thin films grown on $(Sn,Ge)O_2/SnO_2$-buffered sapphire substrates using molecular beam epitaxy (MBE). (b) The substrate temperature (T_s) and pressure (P) map for GeO_2 deposition and the resulting crystallinity of the GeO_2 films. Reproduced from Chae *et al.*, Appl. Phys. Lett. **117**, 072105 (2020) with the permission of AIP Publishing.

stoichiometry of the films [Fig. 5(b)]. The amorphous phase emerges when the adatom mobility is insufficient to enable crystal growth or if the film composition deviates too far from stoichiometry. Meanwhile, high temperatures cause GeO desorption, preventing film growth. The synthesis of single-crystalline r-GeO_2 thin films provides opportunities to experimentally validate its properties for UWBG semiconductor applications.

PERSPECTIVE ON THEORY

First-principles materials' calculations based on the density functional theory and related techniques were instrumental in identifying the desirable dopant and transport features of r-GeO_2 for power-electronics applications. Such atomistic computational methods, which are made available to the research community through well-maintained open-source computer software, have achieved a sufficient level of predictive accuracy to stimulate and guide experimental synthesis and characterization efforts for the discovery of new UWBG semiconductors that advance the current state of the art. For example, the GW method as implemented in, e.g., the BerkeleyGW software[79] predicts accurate band structures, band gaps, effective masses, and dielectric properties of bulk materials and nanostructures. Moreover, the accurate calculations of electron-phonon coupling properties with the density functional perturbation theory in the Quantum ESPRESSO suite of codes and their efficient interpolation for arbitrary wave vectors in the Brillouin zone using maximally localized Wannier functions and the EPW code have enabled accurate and efficient calculations of carrier mobilities through the iterative solution of the Boltzmann transport equation.[80,81] The Boltzmann transport equation applied for phonons with software such as almaBTE can also predict the phonon-limited thermal conductivity of materials.[82] Hybrid-functional calculations have also been instrumental in predicting the defect formation energies and charge-transition levels in a wide range of semiconductors. Future advanced in the computational method and software development will be instrumental in advancing the predictive theoretical characterization of new UWBG semiconductors. For example, techniques to understand carrier scattering by phonons,[83] defects,[84] and alloy disorder,[85] as well as dielectric breakdown phenomena under intense electric fields,[86] as well as the formation of defects and two-dimensional electron/hole gases at semiconductor interfaces[87,88] will be important.

Moreover, first-principles calculations in combination with modern high-performance computing recourses, automated high-throughput calculation execution, open-access materials databases, and materials-informatics techniques can accelerate the discovery of advanced semiconductors through the identification of structural and chemical materials features that give rise to desirable functionalities. For example, the material features that make r-GeO_2 a promising semiconductor for power electronics are (1) its highly symmetric crystal structure, which reduces the modes for electron and phonon scattering and enables high thermal conductivity and mobility, and (2) its dense packing of oxygen anions, which produces a strong overlap of the O 2*p* orbitals and consequently a small hole effective mass that avoids polaron formation, reduces the acceptor activation energy, and enables p-type conductivity. Performing calculations in a systematic fashion can identify more materials with unexpected properties. Similar high-throughput calculations have been successfully applied to discover new p-type transparent conducting materials[89–91] using the band gap and hole effective masses as the screening parameters to predict the competing properties of optical transparency and electrical conductivity. Subsequently, higher-accuracy calculations are performed for the most promising candidates to confirm their desirable band structure, mobility, and dopability. In the field of UWBG semiconductors, Gorai *et al.*[92] performed a broad computational survey to identify materials with a high Baliga figure of merit and a high lattice thermal conductivity using materials–informatics relations (derived from earlier high-throughput calculations) that link the transport properties (mobility and thermal conductivity) and a critical breakdown field to intrinsic material parameters such as dielectric constant, effective mass, phonon cutoff frequency, and bulk modulus. Similar analyses can be deployed to identify candidate UWBG materials with shallow dopants and mobile carriers that can be tested experimentally.

PERSPECTIVES ON SYNTHESIS

On the experimental side, single-crystalline r-GeO_2 thin films have been grown on R-plane sapphire substrates, however, due to the different crystal structure and a large lattice mismatch, defects and dislocations are unavoidably introduced, which degrade carrier mobility and act as a passivation source for free carriers. Homoepitaxy has many advantages for obtaining high-quality films and achieving better device performance. Bulk single crystals of r-GeO_2 have been synthesized through a flux or chemical vapor transport techniques, however,

there are more research opportunities to improve the crystal-quality and the size of r-GeO_2 crystals. From the bulk phase diagram [Fig. 4(a)], the quartz phase solidifies from the melt under ambient pressure, which then presents a challenge to realize large r-GeO_2 single crystals using synthesis techniques such as Czochralski (CZ) or float zone (FZ). The phase stability can be skewed toward the denser rutile phase with applied pressure during the synthesis, which may then allow for the rutile phase to solidify directly from the melt. Prior work on the hydrothermal synthesis of r-GeO_2 has reported a P-T diagram showing that the rutile phase can be synthesized directly from the melt at ~7.6 MPa.[93] Thus, s high pressure FZ or CZ furnaces, such as those at the NSF PARADIM center where up to 30 MPa can be achieved in optical FZ furnaces, may be suitable to stabilize bulk r-GeO_2 single crystals.[94] Large and high-quality crystalline r-GeO_2 substrates would open new doors for the investigation of bulk and thin film electronic properties.

PERSPECTIVES ON DOPING

Controlled doping is one of the most important achievements in semiconductor research. Regarding UWBG semiconductors, the ability to dope is what makes them distinct from insulators and opens device possibilities using junctions; however, as the band gap of material increases, doping becomes more challenging. In the case of wide-band-gap nitrides and oxides such as AlGaN or β-Ga_2O_3, compensating anion vacancies form easily under p-type doping conditions, resulting in the degradation of doping efficiency,[32,95] while the high-lying CBM level of diamond and BN leads to large donor ionization energies.[28] The n- and p-type dopability of r-GeO_2 has only been theoretically predicted so far, and more efforts are required toward the experimental realization of doping in r-GeO_2. The issues with the doping of r-GeO_2 presented by the theory are (1) a relatively deep acceptor level (0.45 eV), which arises from the relatively low-lying valence bands, (2) the formation of compensating defects (e.g., V_O) that are unavoidable under p-type doping conditions, and (3) dislocations or unintentional impurities that are incorporated during synthesis and serve as carrier-trapping centers. However, the doping issues in UWBG semiconductors may be solved by various defect engineering techniques such as co-doping or non-equilibrium growth/processes.

Successful examples of co-doping techniques to improve the doping efficiency include deuteration of boron-doped diamond and hydrogen co-doping of Mg-GaN. The defect complex of H-B-H in diamond has proven to be a more efficient donor compared to single phosphorus defects at room temperature.[96] The enhanced n-doping efficiency is explained by the shift of a donor level to shallower values for the defect complex. Hydrogen co-doping also allows enhanced dopant solubility while suppressing the formation of compensating defects.[97] Due to its amphoteric propensity, the hydrogen interstitial (H_i) easily forms charge-neutral complexes with shallow dopants, while the Coulomb interaction between the H_i and dopant ions reduces the formation energy of the complexes, allowing increased dopant solubility. On the other hand, hydrogen is a fast diffuser and can therefore be effectively removed via a post-annealing treatment in a hydrogen-poor environment to reactivate free carriers. Improved p-type doping efficiency through hydrogen co-doping has been demonstrated for Mg doped GaN and is the key for the fabrication of InGaN LEDs (2014 Nobel Prize in Physics).[98,99] A similar defect-engineering technique can be utilized for the p-doping r-GeO_2 as the incorporation of hydrogen can effectively enhance the solubility of Al acceptors up to ~10^{20} cm^{-3}, while the calculated dissociation energy of Al-H_i (0.96 eV) complexes can be reached by thermal annealing at 700 °C.[30]

Fermi-level engineering is another method to improve the doping efficiency of r-GeO_2. Under equilibrium growth of doped samples, the position of the Fermi level lies close to the band edge, which makes the formation energy of undesirable compensating defects comparable or even lower than the dopants. One solution is to utilize the non-equilibrium growth conditions and shift the Fermi level during synthesis away from the band edge. This can suppress the dopant-defect compensation and enhance the doping efficiency. Such ideas have proven very effective in both p- and n-doping of Al-rich AlGaN alloys.[100,101] In p-type AlGaN, doping with Mg acceptors is severely hampered by the low formation energy of compensating V_N in the conventional epitaxial growth, during which the Fermi level lies near the VBM. However, when the sample is grown at slightly metal (Ga)-rich conditions, a Schottky junction forms at the growth front between the thin Ga metal layer and the AlGaN semiconductor layer during epitaxy, which pins the Fermi level near the middle of the band gap. As a result, the formation energy of Mg acceptors is significantly reduced while the formation energy of compensating V_N increases dramatically. This non-equilibrium junction-assisted epitaxy demonstrates a high hole concentration of ~4.5×10^{17} cm^{-3} in $Al_{0.9}Ga_{0.1}N$.[100] Similarly, the Fermi level control can also be achieved by growing Si-doped AlGaN under above-gap UV illumination. The UV light excites electron–hole pairs and increases the minority hole concentration during the synthesis of n-type AlGaN, which shifts the Fermi level away from the CBM and suppresses the formation of compensating acceptors. This leads to an order of magnitude enhancement in free electron concentration and an improvement of mobility by a factor of 3.[101] These studies demonstrate the promise of creating favorable growth environments for doping with non-equilibrium synthesis techniques, which can also be applied to enhance the doping efficiency of r-GeO_2.

CONCLUSION

The discovery of new materials with enhanced material properties through the synergy of computational and experimental approaches can address the doping limitations of current UWBG semiconductors for power-electronic applications. Here, we have reviewed the theoretical prediction and experimental synthesis of r-GeO_2, an emerging UWBG semiconductor with ambipolar doping, high carrier mobilities, and a higher thermal conductivity than β-Ga_2O_3. The key material parameter that makes r-GeO_2 suitable for energy-efficient power electronics is its highly symmetric and dense crystal structure that induces strong orbital overlaps, which in turn enable small electron and hole effective masses as well as high-lying valence bands that facilitate p-type doping. These features can serve as materials-design principles to computationally discover previously unexplored ambipolarly dopable UWBG semiconductors. We have also discussed the state of the field in terms of the synthesis and characterization of single-crystalline r-GeO_2 in bulk and thin-film forms and highlight that an improved control over defects and dopants is necessary to experimentally realize efficient doping and enable r-GeO_2-based electronics.

ACKNOWLEDGMENTS

The theoretical work was supported by the National Science Foundation through the Designing Materials to Revolutionize and

Engineer our Future (DMREF) Program under Award No. 1534221 (band structure, doping, and defect theory) and by the Computational Materials Sciences Program funded by the U.S. Department of Energy, Office of Science, Basic Energy Sciences under Award No. DE-SC0020129 (phonons, mobility, and thermal-transport theory). The experimental work was supported by the National Science Foundation Award No. DMR 1810119 (bulk and thin film synthesis and structural characterization), by the U.S. Department of Energy, Office of Science, Basic Energy Sciences under Award No. DE-SC00018941 (bulk thermal transport measurements by the National Science Foundation) [Platform for the Accelerated Realization, Analysis, and Discovery of Interface Materials (PARADIM)] under Cooperative Agreement No. DMR-1539918 (thin-film synthesis and characterization), and by the NSF CAREER Grant No. DMR-1847847 (perspective on synthesis). K.B. acknowledges the support of the DOE Computational Science Graduate Fellowship Program through Grant No. DE-SC0020347.

DATA AVAILABILITY

Data sharing is not applicable to this article as no new data were created or analyzed in this study.

REFERENCES

[1]J. Y. Tsao, S. Chowdhury, M. A. Hollis, D. Jena, N. M. Johnson, K. A. Jones, R. J. Kaplar, S. Rajan, C. G. van de Walle, E. Bellotti, C. L. Chua, R. Collazo, M. E. Coltrin, J. A. Cooper, K. R. Evans, S. Graham, T. A. Grotjohn, E. R. Heller, M. Higashiwaki, M. S. Islam, P. W. Juodawlkis, M. A. Khan, A. D. Koehler, J. H. Leach, U. K. Mishra, R. J. Nemanich, R. C. N. Pilawa-Podgurski, J. B. Shealy, Z. Sitar, M. J. Tadjer, A. F. Witulski, M. Wraback, and J. A. Simmons, Adv. Electron. Mater. **4**, 1600501 (2018).
[2]M. Higashiwaki, K. Sasaki, A. Kuramata, T. Masui, and S. Yamakoshi, Appl. Phys. Lett. **100**, 013504 (2012).
[3]S. M. Sze and K. K. Ng, *Physics of Semiconductor Devices*, 3rd ed. (John Wiley & Sons, Hoboken, NJ, 2006).
[4]B. J. Baliga, *Fundamentals of Power Semiconductor Devices* (Springer Science & Business Media, Berlin, 2010).
[5]J. M. Dorkel and P. Leturcq, Solid State Electron. **24**, 821 (1981).
[6]M. Levinstein, S. Rumyantsev, and M. Shur, *Handbook Series on Semiconductor Parameters* (World Scientific, London, 1996), Vol. 1.
[7]K. Bushick, K. A. Mengle, S. Chae, and E. Kioupakis, Appl. Phys. Lett. **117**, 182104 (2020).
[8]M. E. Levinstein, S. L. Rumyantsev, and M. S. Shur, *Properties of Advanced Semiconductor Materials: GaN, AlN, InN, BN, SiC, SiGe* (John Wiley & Sons, Hoboken, NJ, 2001).
[9]A. A. Lebedev, Semiconductors **33**, 107 (1999).
[10]A. S. Barker and M. Ilegems, Phys. Rev. B **7**, 743 (1973).
[11]M. Horita, S. Takashima, R. Tanaka, H. Matsuyama, K. Ueno, M. Edo, T. Takahashi, M. Shimizu, and J. Suda, Jpn. J. Appl. Phys. **56**, 031001 (2017).
[12]S. Strite, J. Vac. Sci. Technol. B Microelectron. Nanom. Struct. **10**, 1237 (1992).
[13]K. Sasaki, A. Kuramata, T. Masui, E. G. Víllora, K. Shimamura, and S. Yamakoshi, Appl. Phys. Express **5**, 035502 (2012).
[14]Z. Feng, A. F. M. Anhar Uddin Bhuiyan, M. R. Karim, and H. Zhao, Appl. Phys. Lett. **114**, 250601 (2019).
[15]L. Binet and D. Gourier, J. Phys. Chem. Solids **59**, 1241 (1998).
[16]A. Kyrtsos, M. Matsubara, and E. Bellotti, Appl. Phys. Lett. **112**, 032108 (2018).
[17]Z. Guo, A. Verma, X. Wu, F. Sun, A. Hickman, T. Masui, A. Kuramata, M. Higashiwaki, D. Jena, and T. Luo, Appl. Phys. Lett. **106**, 111909 (2015).
[18]A. T. Collins, E. C. Lightowlers, and P. J. Dean, Phys. Rev. **158**, 833 (1967).
[19]Y. Taniyasu, M. Kasu, and T. Makimoto, Appl. Phys. Lett. **89**, 182112 (2006).
[20]J. Edwards, K. Kawabe, G. Stevens, and R. H. Tredgold, Solid State Commun. **3**, 99 (1965).
[21]Y. Taniyasu, M. Kasu, and T. Makimoto, Appl. Phys. Lett. **85**, 4672 (2004).
[22]G. A. Slack, R. A. Tanzilli, R. O. Pohl, and J. W. Vandersande, J. Phys. Chem. Solids **48**, 641 (1987).
[23]A. Soltani, A. Talbi, V. Mortetb, A. Benmoussa, W. J. Zhang, J. C. Gerbedoen, J. C. de Jaeger, A. Gokarna, K. Haenen, and P. Wagner, AIP Conf. Proc. **1292**, 191 (2010).
[24]D. Litvinov, C. A. Taylor, and R. Clarke, Diam. Relat. Mater. **7**, 360 (1998).
[25]H. Murata, T. Taniguchi, S. Hishita, T. Yamamoto, F. Oba, and I. Tanaka, J. Appl. Phys. **114**, 233502 (2013).
[26]L. Weston, D. Wickramaratne, and C. G. van de Walle, Phys. Rev. B **96**, 100102(R) (2017).
[27]K. Chen, B. Song, N. K. Ravichandran, Q. Zheng, X. Chen, H. Lee, H. Sun, S. Li, G. A. G. U. Gamage, F. Tian, Z. Ding, Q. Song, A. Rai, H. Wu, P. Koirala, A. J. Schmidt, K. Watanabe, B. Lv, Z. Ren, L. Shi, D. G. Cahill, T. Taniguchi, D. Broido, and G. Chen, Science **367**, 555 (2020).
[28]N. Donato, N. Rouger, J. Pernot, G. Longobardi, and F. Udrea, J. Phys. D. Appl. Phys. **53**, 093001 (2020).
[29]D. M. Roessler and W. A. Albers, J. Phys. Chem. Solids **33**, 293 (1972).
[30]S. Chae, J. Lee, K. A. Mengle, J. T. Heron, and E. Kioupakis, Appl. Phys. Lett. **114**, 102104 (2019).
[31]S. Chae, K. A. Mengle, R. Lu, A. Olvera, N. Sanders, J. Lee, P. F. P. Poudeu, J. T. Heron, and E. Kioupakis, Appl. Phys. Lett. **117**, 102106 (2020).
[32]C. G. van de Walle, C. Stampfl, J. Neugebauer, M. D. McCluskey, and N. M. Johnson, MRS Internet J. Nitride Semicond. Res **4**, 890 (1999).
[33]Y. Liang and E. Towe, Appl. Phys. Rev. **5**, 011107 (2018).
[34]J. B. Varley, A. Janotti, C. Franchini, and C. G. van de Walle, Phys. Rev. B **85**, 081109(R) (2012).
[35]M.-A. Pinault, J. Barjon, T. Kociniewski, F. Jomard, and J. Chevallier, Physics B **401-402**, 51 (2007).
[36]J. P. Goss, P. R. Briddon, M. J. Rayson, S. J. Sque, and R. Jones, Phys. Rev. B **72**, 035214 (2005).
[37]N. Izyumskaya, D. O. Demchenko, S. Das, Ü. Özgür, V. Avrutin, and H. Morkoc, Adv. Electron. Mater. **3**, 1600485 (2017).
[38]A. Goyal and V. Stevanović, Phys. Rev. Mater. **2**, 084603 (2018).
[39]C. P. Liu, K. O. Egbo, C. Y. Ho, Y. Wang, C. K. Xu, and K. M. Yu, Phys. Rev. Appl. **13**, 024049 (2020).
[40]Z. Galazka, S. Ganschow, R. Schewski, K. Irmscher, D. Klimm, A. Kwasniewski, M. Pietsch, A. Fiedler, I. Schulze-Jonack, M. Albrecht, T. Schröder, and M. Bickermann, APL Mater. **7**, 022512 (2019).
[41]E. Chikoidze, C. Sartel, I. Madaci, H. Mohamed, C. Vilar, B. Ballesteros, F. Belarre, E. del Corro, P. Vales-Castro, G. Sauthier, L. Li, M. Jennings, V. Sallet, Y. Dumont, and A. Pérez-Tomás, Cryst. Growth Des. **20**, 2535 (2020).
[42]S. K. Radha, A. Ratnaparkhe, and W. R. L. Lambrecht, Phys. Rev. B **103**, 045201 (2021).
[43]K. Dabsamut, A. Boonchun, and W. R. L. Lambrecht, J. Phys. D. Appl. Phys. **53**, 274002 (2020).
[44]A. Boonchun, K. Dabsamut, and W. R. L. Lambrecht, J. Appl. Phys. **126**, 155703 (2019).
[45]M. Micoulaut, L. Cormier, and G. S. Henderson, J. Phys. Condens. Matter **18**, R753 (2006).
[46]A. W. Laubengayer and D. S. Morton, J. Am. Chem. Soc. **54**, 2303 (1932).
[47]M. Sahnoun, C. Daul, R. Khenata, and H. Baltache, Eur. Phys. J. B **45**, 455 (2005).
[48]Q. Liu, Z. Liu, L. Feng, and H. Tian, Solid State Sci. **12**, 1748 (2010).
[49]K. A. Mengle, S. Chae, and E. Kioupakis, J. Appl. Phys. **126**, 085703 (2019).
[50]A. Samanta, M. Jain, and A. K. Singh, J. Chem. Phys. **143**, 064703 (2015).
[51]M. Stapelbroek and B. D. Evans, Solid State Commun. **25**, 959 (1978).
[52]N. Ma, N. Tanen, A. Verma, Z. Guo, T. Luo, H. (Grace) Xing, and D. Jena, Appl. Phys. Lett. **109**, 212101 (2016).
[53]H. Peelaers and C. G. van de Walle, Phys. Rev. B **96**, 081409(R) (2017).
[54]M. Feneberg, C. Lidig, K. Lange, M. E. White, M. Y. Tsai, J. S. Speck, O. Bierwagen, and R. Goldhahn, Phys. Status Solidi A **211**, 82 (2014).
[55]Q. Yan, E. Kioupakis, D. Jena, and C. G. van de Walle, Phys. Rev. B **90**, 121201(R) (2014).
[56]K. A. Mengle, G. Shi, D. Bayerl, and E. Kioupakis, Appl. Phys. Lett. **109**, 212104 (2016).

[57]C. A. Niedermeier, K. Ide, T. Katase, H. Hosono, and T. Kamiya, J. Phys. Chem. C **124**, 25721 (2020).
[58]D. O. Scanlon and G. W. Watson, J. Mater. Chem. **22**, 25236 (2012).
[59]K. Bushick, K. Mengle, N. Sanders, and E. Kioupakis, Appl. Phys. Lett. **114**, 022101 (2019).
[60]V. V. Brazhkin, A. G. Lyapin, R. N. Voloshin, S. V. Popova, E. V. Tat'yanin, N. F. Borovikov, S. C. Bayliss, and A. V. Sapelkin, Phys. Rev. Lett. **90**, 145503 (2003).
[61]V. V. Brazhkin, E. V. Tat'yanin, A. G. Lyapin, S. V. Popova, O. B. Tsiok, and D. V. Balitskiĭ, JETP Lett. **71**, 293 (2000).
[62]J. Haines, J. Léger, and C. Chateau, Phys. Rev. B **61**, 8701 (2000).
[63]S. Kawasaki, O. Ohtaka, and T. Yamanaka, Phys. Chem. Miner. **20**, 531 (1994).
[64]V. Agafonov, D. Michel, M. Perez, Y. Jorba, and M. Fedoroff, Mater. Res. Bull. **19**, 233 (1984).
[65]J. W. Goodrum, J. Cryst. Growth **7**, 254 (1970).
[66]T. Bielz, S. Soisuwan, R. Kaindl, R. Tessadri, D. M. Többens, B. Klötzer, and S. Penner, J. Phys. Chem. C **115**, 9706 (2011).
[67]C. Caperaa, G. Baud, J. P. Besse, P. Bondot, P. Fessler, and M. Jacquet, Mater. Res. Bull. **24**, 1361 (1989).
[68]N. R. Murphy, J. T. Grant, L. Sun, J. G. Jones, R. Jakubiak, V. Shutthanandan, and C. V. Ramana, Opt. Mater. (Amst). **36**, 1177 (2014).
[69]A. Chiasera, C. Macchi, S. Mariazzi, S. Valligatla, L. Lunelli, C. Pederzolli, D. N. Rao, A. Somoza, R. S. Brusa, and M. Ferrari, Opt. Mater. Express **3**, 1561 (2013).
[70]N. Terakado and K. Tanaka, J. Non-Cryst. Solids **351**, 54 (2005).
[71]P. J. Wolf, T. M. Christensen, N. G. Coit, and R. W. Swinford, J. Vac. Sci. Technol. A **11**, 2725 (1993).
[72]S. Witanachchi and P. J. Wolf, J. Appl. Phys. **76**, 2185 (1994).
[73]C. N. Afonso, F. Vega, J. Solis, F. Catalina, C. Ortega, and J. Siejka, Appl. Surf. Sci. **54**, 175 (1992).
[74]J. Beynon, M. M. E. Samanoudy, and E. L. Shorts, J. Mater. Sci. **23**, 4363 (1988).
[75]S. Chae, H. Paik, N. M. Vu, E. Kioupakis, and J. T. Heron, Appl. Phys. Lett. **117**, 072105 (2020).
[76]J. H. Kwon, Y. H. Choi, D. H. Kim, M. Yang, J. Jang, T. W. Kim, S. H. Hong, and M. Kim, Thin Solid Films **517**, 550 (2008).
[77]J. Lu, J. Sundqvist, M. Ottosson, A. Tarre, A. Rosental, J. Aarik, and A. Hårsta, J. Cryst. Growth **260**, 191 (2004).
[78]J. Sundqvist, J. Lu, M. Ottosson, and A. Hårsta, Thin Solid Films **514**, 63 (2006).
[79]J. Deslippe, G. Samsonidze, D. A. Strubbe, M. Jain, M. L. Cohen, and S. G. Louie, Comput. Phys. Commun. **183**, 1269 (2012).
[80]S. Poncé, E. R. Margine, C. Verdi, and F. Giustino, Comput. Phys. Commun. **209**, 116 (2016).
[81]J. Noffsinger, F. Giustino, B. D. Malone, C. H. Park, S. G. Louie, and M. L. Cohen, Comput. Phys. Commun. **181**, 2140 (2010).
[82]J. Carrete, B. Vermeersch, A. Katre, A. van Roekeghem, T. Wang, G. K. H. Madsen, and N. Mingo, Comput. Phys. Commun. **220**, 351 (2017).
[83]F. Giustino, Rev. Mod. Phys. **89**, 015003 (2017).
[84]I. Lu, J. Zhou, and M. Bernardi, Phys. Rev. Mater. **3**, 033804 (2019).
[85]S. Fahy, A. Lindsay, H. Ouerdane, and E. P. O'Reilly, Phys. Rev. B **74**, 035203 (2006).
[86]K. Ghosh and U. Singisetti, J. Appl. Phys. **124**, 085707 (2018).
[87]R. Chaudhuri, S. J. Bader, Z. Chen, D. A. Muller, H. G. Xing, and D. Jena, Science **365**, 1454 (2019).
[88]J. P. Ibbetson, P. T. Fini, K. D. Ness, S. P. DenBaars, J. S. Speck, and U. K. Mishra, Appl. Phys. Lett. **77**, 250 (2000).
[89]G. Hautier, A. Miglio, G. Ceder, G. Rignanese, and X. Gonze, Nat. Commun. **4**, 2292 (2013).
[90]G. Brunin, F. Ricci, V.-A. Ha, G.-M. Rignanese, and G. Hautier, NPJ Comput. Mater. **5**, 63 (2019).
[91]R. Woods-Robinson, D. Broberg, A. Faghaninia, A. Jain, S. S. Dwaraknath, and K. A. Persson, Chem. Mater. **30**, 8375 (2018).
[92]P. Gorai, R. W. McKinney, N. M. Haegel, A. Zakutayev, and V. Stevanovic, Energy Environ. Sci. **12**, 3338 (2019).
[93]V. G. Hill and L. L. Y. Chang, Am. Mineral. **53**, 1744 (1968).
[94]See https://www.paradim.org/ for information about PARADIM's facilities for bulk crystal and thin film growth.
[95]E. Chikoidze, A. Fellous, A. Perez-Tomas, G. Sauthier, T. Tchelidze, C. Ton-That, T. Thanh, M. Phillips, S. Russell, M. Jennings, B. Berini, F. Jomard, and Y. Dumont, Mater. Today Phys. **3**, 118 (2017).
[96]Z. Teukam, J. Chevallier, C. Saguy, R. Kalish, D. Ballutaud, M. Barbé, F. Jomard, A. Tromson-Carli, C. Cytermann, J. E. Butler, M. Bernard, C. Baron, and A. Deneuville, Nat. Mater. **2**, 482 (2003).
[97]C. G. van der Walle and J. Neugebauer, Annu. Rev. Mater. Res. **36**, 179 (2006).
[98]J. Neugebauer and C. G. van de Walle, Appl. Phys. Lett. **68**, 1829 (1996).
[99]S. Nakamura, N. Iwasa, M. Senoh, and T. Mukai, Jpn. J. Appl. Phys. **31**, 1258 (1992).
[100]A. Pandey, X. Liu, Z. Deng, W. J. Shin, D. A. Laleyan, K. Mashooq, E. T. Reid, E. Kioupakis, P. Bhattacharya, and Z. Mi, Phys. Rev. Mater. **3**, 053401 (2019).
[101]Z. Bryan, I. Bryan, B. E. Gaddy, P. Reddy, L. Hussey, M. Bobea, W. Guo, M. Hoffmann, R. Kirste, J. Tweedie, M. Gerhold, D. L. Irving, Z. Sitar, and R. Collazo, Appl. Phys. Lett. **105**, 222101 (2014).